Technology Advances in GNSS High Precision Positioning Antennas

D. V. Tatarnikov
Topcon Positioning Systems, Russia

Abstract— Typical error of high precision positioning with the Global Navigation Satellite Systems (GNSS) is currently about $+/-1\dots2$ cm in real time; multipath reflections from the Earth surface underlaying the receiver antenna is the largest error source. Newly developed compact low-loss rover antennas and reference station antennas are presented. The developed antennas with cutoff pattern potentially bring the millimeter precision in "almost" real time to the realm of practice. With the antennas, precision achieved is estimated to be of 0.65 mm in rms sense given phase noise of the system smoothed out within a time interval of 1 minute span.

1. INTRODUCTION

Currently, typical error of high precision positioning with the Global Navigation Satellite Systems (GNSS) is of the order of $+/-1\dots2$ cm in real time and of $1\dots2$ mm in post-processing. The technique is widely used in various areas of business and research. A high precision system processes a variety of the GNSS signals along with certain types of corrections [1]. However, even with the best open sky sites there remains a site-dependent error associated with the reflections of satellite signals from the earth surface undelaying the user antenna. The reflections are referred to as multipath and are the major contribution to the total error of positioning. The way to mitigate the error is a proper shaping of the receiving antenna pattern.

From antenna technology standpoint the GNSS spectrum is a plurality of two sub-bands: the Lower GNSS band (1160–1300 MHz) and the Upper GNSS band ($1540\dots1610$ MHz). The antennas are to receive right-hand circular polarized (RHCP) signals. One would mention that the increase of the antenna noise temperature largely contributes to malfunctioning the phase lock loops (PLL) of the receiver. This differentiates the high precision equipment from other branches of satellite positioning where the delay lock loop is of interest. Thus, the art of the antenna design is to provide with compact low loss antennas. An ideal antenna for high precision applications would have +3 dB gain for all the directions in top semi-sphere and 0 gain for the directions underneath. This is to mitigate the reflections. In practice, antenna gain roll-off from zenith to horizon of about $10\dots15$ dB is viewed as acceptable. Larger roll-offs normally are associated with the PLL malfunctioning, in particular in regards to low elevated satellites. The desire to approach the step-like pattern yet keeping antennas to practical size is one of the major directions in antenna developments. Last but not least, cost efficiency is a factor.

It is practical to characterize antennas by the down up ratio $DU(\theta^e) = F(-\theta^e)/F(\theta^e)$. Here $F(\pm\theta^e)$ is the antenna pattern reading for a certain angle θ^e above (below) the local horizon. Within the specular reflections model, the ratio gives the multipath error to positioning [1]. Typical plots approximated by linear trends are shown in Fig. 1. The curve 1 is for the so-called rovers, i.e., antennas for practical use in the field. This kind of behavior allows to achieve the precision in real time mentioned above. The curve 2 is for base stations. Here, mm-level precision in post-processing is achievable. Finally, the curve 3 is for "no-multipath" antenna which would be required for millimeter precision is real time. In regards to the latter one would mention that normally satellites below 10 degrees elevation are omitted during processing. This is due to a large degree of distortion of their signals by natural or human-made obstacles. Thus, "no multipath" antenna would have about 40 dB drop of the gain (cutoff) within $+/-10$ degrees angular sector.

This paper is an overview of results and perspectives of the developments done in Technology Center of Topcon Corp. in Moscow, Russia. Books [2, 3] could be recommended for a broader view of the GNSS receiving antenna technology.

2. PATCH ANTENNAS WITH ARTIFICIAL DIELECTRIC SUBSTRATES

Given an acceptable roll-off of the gain from zenith to horizon of above, a common patch antenna is to have a dielectric substrate with relative permittivity equal to about four [1]. Then, antenna Q-factor estimates [4] show that the required bandwidth claims for the substrate thickness to be of about 1 cm or more. Dense low-loss substrates of such thickness contribute to antenna weight increase and manufacturing complications. As an alternative, patch antennas with substrates made

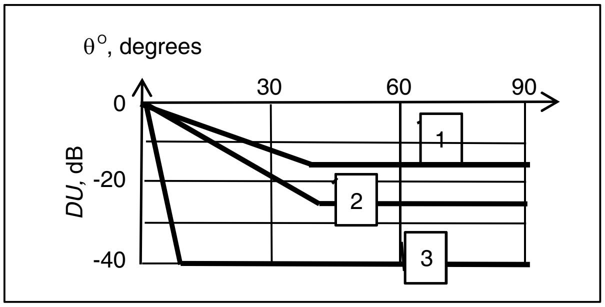

Figure 1: Down-up ratio versus satellite elevation.

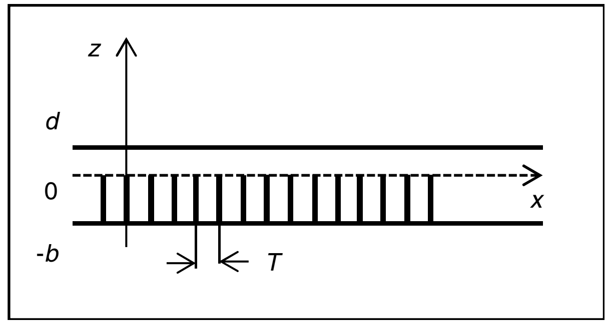

Figure 2: Parallel-plate waveguide filled with a structure of ribs.

Figure 3: Dual band patch antenna with comb substrates.

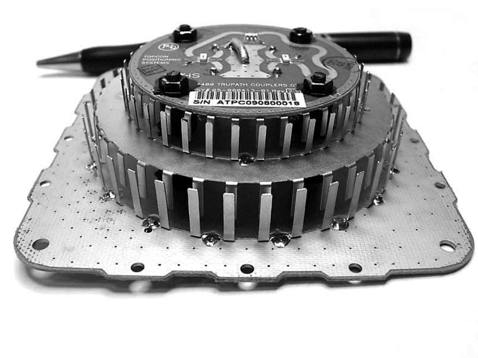

Figure 4: Dual band patch antenna with capacitive frame.

of light weight metal structures have been considered [5, 6]. Basics of the approach are illustrated as follows.

Consider a parallel-plate waveguide partially filled with the structure of metal ribs located at $-b < z < 0$ (Fig. 2). For $T \ll \lambda$, let the ribs form an averaged inductive surface impedance $Z_S = i\eta_0 tg(kd)$ (with k being a wavenumber, λ being a wavelength, η_0 being an intrinsic impedance, all of free space, and i being an imaginary unit). Then, for b, $d \ll \lambda$ the slowdown factor β of the wave propagating in x direction in the area $0 < z < d$ is $\beta = \sqrt{\varepsilon_{eff}} = \sqrt{1 + b/d}$ [7]. Here ε_{eff} is equivalent effective dielectric permittivity. Thus, for small enough d a high ε_{eff} potentially could be actualized. For circular polarized antennas one is interested in a structure of thin pins rather than ribs. More accurate estimates [5] show that $\varepsilon_{eff} \approx 4$ is achievable. Fig. 3 illustrates a dual-band patch antenna stack [8]. The antenna has been used for navigation of automated machines in agriculture and construction.

Further on, with TM_{10} cavity mode of a patch antenna, the electric field intensity in the area near the antenna center of symmetry is small. This suggests that pins of the central area could be removed. This has led to the patch stack design with substrates in the form of a capacitive frame [9]. The sample is shown in Fig. 4. The weight of this stack is 150 gram.

One would mention that the estimates [6] show that a capacitive frame potentially offers a slight bandwidth increase versus a regular dielectric. The way to estimate ε_{eff} is like follows. Consider a linear polarized squared patch antenna furnished with such a frame (Fig. 5). For a wave propagating in between a patch and a ground plane in the x-direction an equivalent longitudinal chain circuit of Fig. 6(a) holds. Here, the characteristic impedance $W = \eta_0 h/a$ is taken as that of the cut of a parallel-plate waveguide filled with air with width a equal to the patch size and height h equal to the substrate thickness. Let B_{C1} be the susceptance of capacitors per one period of the longitudinal structure 1 (Fig. 5) and β_1 be the an equivalent slowdown factor of the structure. For $T \ll \lambda$ and not too big β_1, for the chain of Fig. 6(a)) the expression $\beta_1 = \sqrt{1 + (B_{C1}W/kT)}$ holds [10].

Next, consider an equivalent circuit of a patch antenna in the form of a quarter-wave stub (Fig. 6(b)). Here G_Σ is the admittance [4], B_{C2} is the total susceptance of transversal structure 2 of Fig. 5. It is assumed that the stub is filled with a homogeneous medium with slowdown factor

β_1 of above; thus, the characteristic impedance is $W_1 = \eta_0 h/(\beta_1 a)$. The resonant condition for the stub is $B_{C2}W_1 = ctg(k\beta_1 a/2)$. For the circular polarized antenna, the structures 1 and 2 are identical. Writing B_C for the susceptance of one capacitor one has $B_{C1} = 2B_C$, $B_{C2} = B_C a/T$. Let $\alpha = B_C\eta_0 h/T$ be the constitutive parameter of the substrate. Then, one has a system of two equations $\beta_1 = \sqrt{1 + (2\alpha/ka)}$; $\alpha = \beta_1 ctg(k\beta_1 a/2)$. The equations define the resonant size a as a function of α. Effective permittivity of the substrate ε_{eff} is then introduced by writing $\beta = \sqrt{\varepsilon_{eff}} = \lambda/(2a)$. A convenient way to solve the equations could be seen in [1].

With some applications the Lower GNSS band narrows to 1215 . . . 1260 MHz. This is the so-called dual frequency $L1/L2$ functionality. Then, a compact concentric dual band patch antenna could be considered rather than a stack. The concentric antenna introduced by late 90-s employing ceramic substrate is shown in [1]. In Fig. 7 a version with a metal capacitive substrate is illustrated. The inner patch is for $L1$ band and the outer is for $L2$. The antenna has weight of 90 gram.

3. COMPACT MULTIPATH-PROTECTED ROVER ANTENNAS

The antennas are to meet the curve 1 of Fig. 1. For the purpose, a patch antenna onto a flat metal ground plane is the most common arrangement. Estimates [1] show that the minimal acceptable ground plane size is about half-the wavelength. With the ground plane of lesser size, the antenna multipath rejection capability degrades. To overcome the limit, an anti-antenna approach has been suggested [11]. The approach could be illustrated as follows. Consider a two-dimensional model in the form of two parallel magnetic line currents arranged into a stack with respect to the vertical z-axis such that $\vec{j}^{\,m}_{1,2} = U_{1,2}\delta(z \mp d)\vec{x}_0$. Here $U_{1,2}$ are magnitudes of voltages across the currents, $\delta(z \mp d)$ are the Dirac delta-functions, $\vec{x}_0$ is the unit vector of Cartesian frame, $d \ll \lambda$. If $U_2 = -U_1 \exp(-2ikd)$ then the pattern in the z-y plane is a cardioid with radiation downward suppressed. Now consider two patch antennas arranged in a vertical stack (see Fig. 8; the top antenna 1 has a ceramic substrate and the bottom antenna 2 has a comb metal substrate of above. A low-noise amplifier 3 is arranged atop the antenna 1). The top patch antenna is active

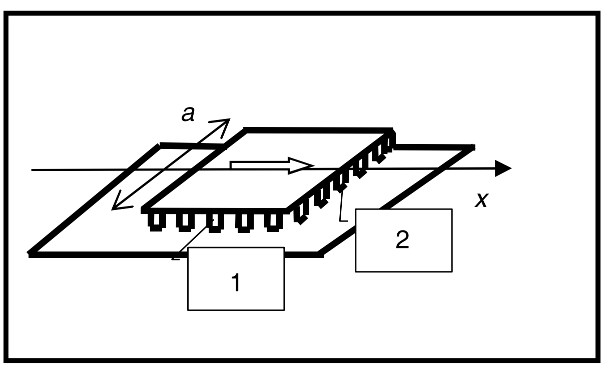

Figure 5: Linear polarized patch antenna with capacitive frame.

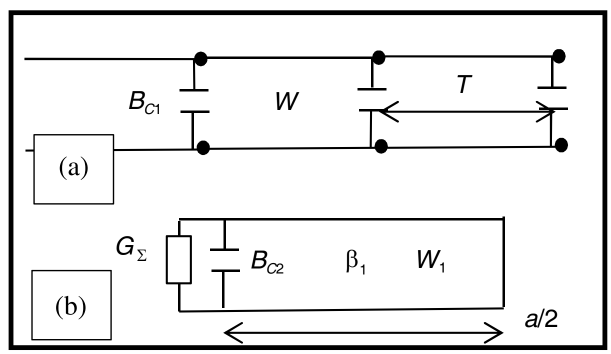

Figure 6: Longitudinal and transverse equivalent circuits.

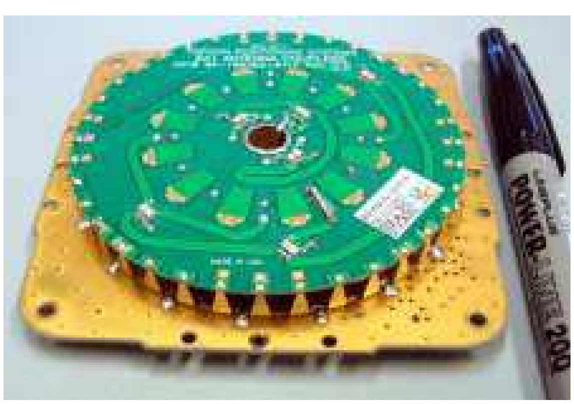

Figure 7: Concentric $L1/L2$ antenna.

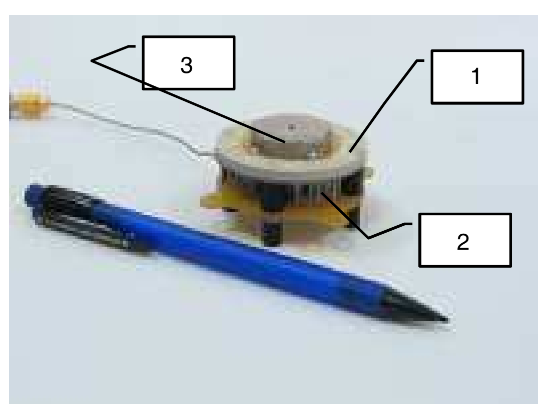

Figure 8: Implementation of anti-antenna concept.

and the bottom patch antenna is passive and tuned such that the just described relationship of voltages across the radiating slots of the two antennas holds. The bottom patch is called the anti-antenna [12]. The antenna stack does not require a ground plane. Compared to flat metal ground plane, size reduction in horizontal plane by a factor of $\sqrt{\varepsilon_{eff}}$ is achieved. Here ε_{eff} is the effective permittivity of the substrate. The details and examples of dual band quadri-patch structures could be seen in [1, 12, 13]. The approach has been employed in a design of compact positioning units (sensors) [14]. As an example, the left panel in Fig. 9 illustrates an antenna stack and the anti-antenna arranged atop the housing with receiver electronics. Measured antenna patterns are shown at the right panel. With the design,the down-up ratio in nadir direction (at 180°) exceeds 15 dB in absolute value.

Another type of compact antennas not requiring a ground plane for multipath protection is helices. Helix antennas have been employed for satellite positioning since the beginning in late 1980-s (see [2, 15] and references therein). With compact designs, sufficient bandwidth is a topic for further developments. As an example of the newly done developments, Fig. 10(a) illustrates the dual-band quadrifilar helix antenna compatible with GPS, GLONASS, Gelileo and BeiDou satellite systems. The type of the pattern achieved is illustrated at the right panel of the figure.

We complete this Section with the remark that by constructing a linear combination of spherical harmonics one is able to achieve a pattern of the kind of $\exp(-i\varphi)(dP_n^1(\cos\theta)/d\theta + P_n^1(\cos\theta)/\sin\theta)$ $(\vec{\theta}_0 - i\vec{\varphi}_0)$. Here θ, φ are the zenith angle and azimuth, respectively, $\vec{\theta}_0$, $\vec{\varphi}_0$ are the unit vectors of a spherical coordinate frame, $P_n^1(\cos\theta)$ is the Legendre function of the n-th order. The pattern has only a RHCP component within the entire sphere thus with radiation downwards suppressed. This type of pattern could be achieved by a pair of magnetic m and electric e current rings coinciding with each other. In spherical coordinates, $\vec{j}^{e,m} = \vec{\varphi}_0 I^{e,m} \exp(-i\varphi)\delta(r-a)\delta(\theta-\pi/2)/r$ with the magnitudes obeying $I^m = i\eta_0 I^e$. With small enough a a perfect cardioid pattern is realized. An

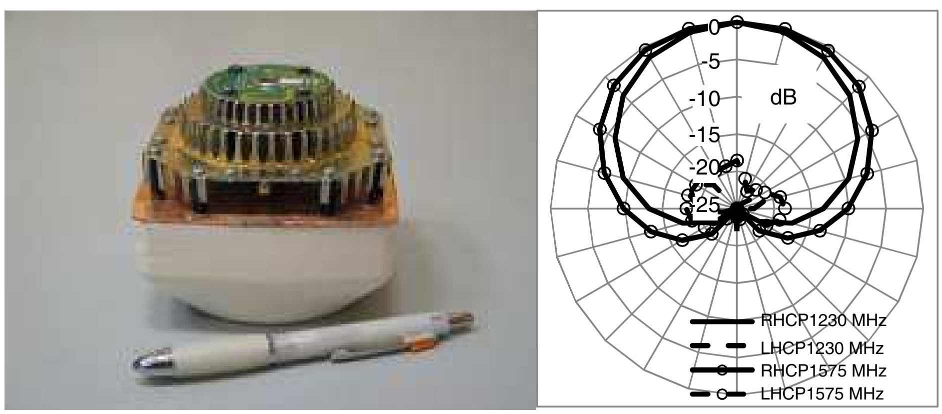

(a) (b)

Figure 9: Integrated sensor of position.

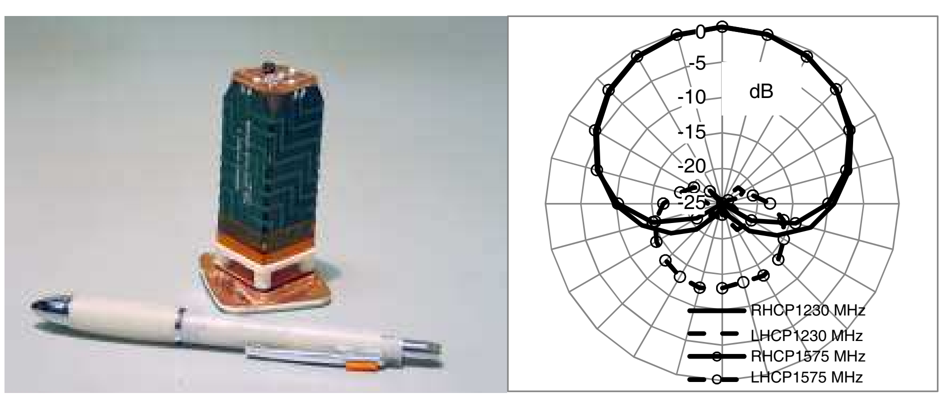

(a) (b)

Figure 10: Dual band helix antenna.

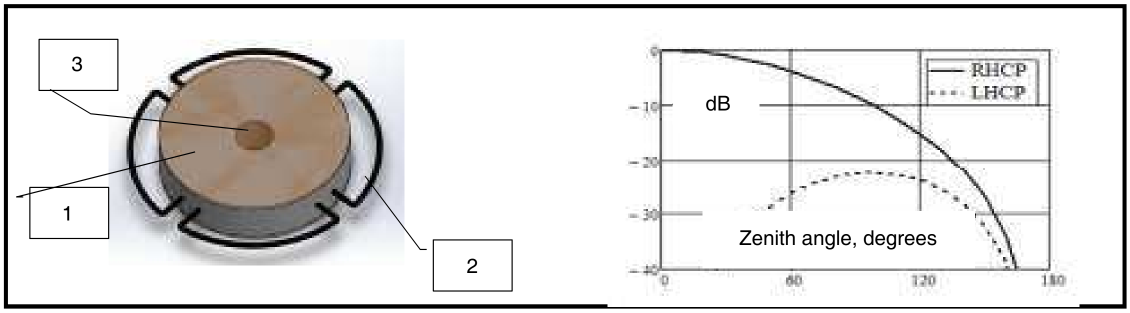

(a) (b)

Figure 11: Symmetrical patch antenna combined with a loop antenna.

example of the respective structure is shown in Fig. 11(a). Here 1 is a symmetrical patch antenna, 2 is a wire loop antenna. Power combiner 3 is located at the center of the patch antenna. Calculations with the CST software have shown that at the distance between the patch and the loop of the order of hundredths of the wavelength, the two antennas are de-coupled due to geometrical and electrical symmetry. The calculated pattern is shown at the right panel of Fig. 11. Here, the cross-polarized (LHCP) component does not exceed −20 dB with the down-up ratio in nadir direction exceeding 40 dB in absolute value. The size of the structure is about 1/4 of the wavelength.

4. REFERENCE STATION ANTENNAS

The antennas generally meet the curve 2 of Fig. 1. The most common example is a Choke Ring ground plane antenna serving for geodetic community for more than 20 years. See [16] for the basics of design and [1] for a photopicture and antenna patterns. The Choke Ring ground plane realizes a high capacitive impedance surface. However, a natural feature of such surfaces is antenna pattern narrowing. One would mention that with two dimensional approximation and large enough ground plane, an antenna pattern null in the direction grazing the ground plane is formed. This is well-known, details could checked in [12]. Said narrowing affects the ability of the antenna to support tracking of low elevated satellites. With the goal of widening the pattern while not affecting the multipath rejection capabilities of an antenna, a non-planar pyramidal structure has been suggested [17]. The approach of [18, 19] could be illustrated as follows.

Consider two magnetic ring currents placed at a small distance from each other (Fig. 12(a)). The currents obey $\exp(-i\varphi)$ behavior versus azimuth, the magnitudes of the two currents are related such that to approach a cardioid pattern in the elevation plane. The currents are to model radiation of a circular polarized antenna arranged atop a ground plane. Let the ground plane (a dotted line in Fig. 12(a)) be of a spherical shape and realize a perfect magnetic conductor (PMC) boundary. Then, as discussed in [18], with small enough R the radiation pattern approaches that of the currents in free space. However, with R increases within a practically reasonable range, the antenna gain for low elevations stays almost unchanged while the radiation in the direction downwards decreases rapidly. This has served as a base for designing an antenna shown at the right panel of the figure. Here, a PMC surface is realized by a straight pins structure. The antenna has a larger gain in the directions of low elevated satellites versus a common Choke Ring ground plane while having the same multipath protection. Other details of the design could be checked in [1, 18]. The internal volume of the antenna is utilized to accommodate high-Q cavity filters for interference suppression.

Another type is the so-called field reference station antennas. The antennas are intended for practical applications in the field environment and are to provide with the precision competitive to those for the reference stations while having less weight and size. Potentials to control the radiation pattern by semi-transparent ground planes with complex grid impedance have been discussed in [20]. With antenna shown in Fig. 13(a) the semi-transparency is achieved by a slot loaded by a system of complex impedances. The radiating pattern of the antenna is illustrated in Fig. 13(a). Here the antenna gain roll-off from zenith to horizon is 10 . . . 13 dB while the down/up ratio in nadir direction is −25 dB. One of the features of the field reference station antennas is decreased intensity of the near-fields in the region underneath. This is to reduce the errors in positioning associated with metal objects which normally appear with practical setups. In geodetic literature, the errors are referred to as near-field effects [21]. Fig. 13(c) illustrates the test setup with a metal disk

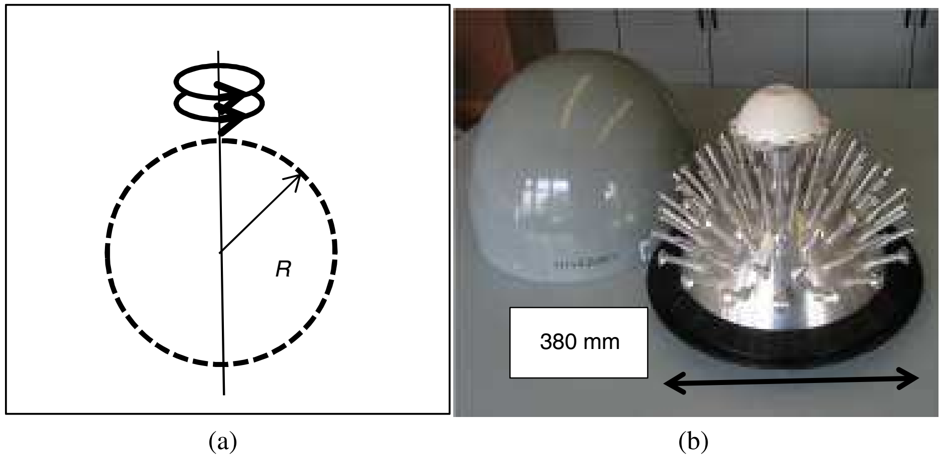

Figure 12: Reference station antenna with convex impedance ground plane.

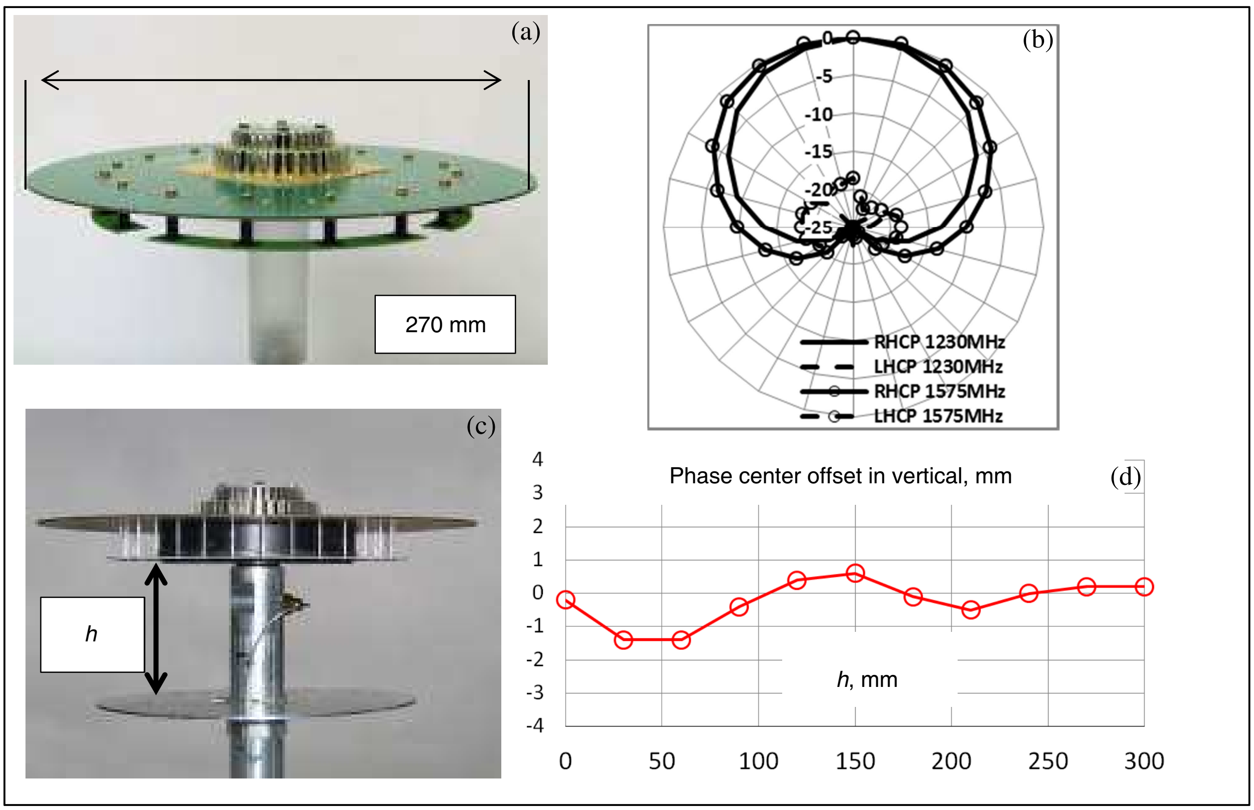

Figure 13: Field reference station antenna with semi-transparent ground plane.

underneath the antenna. Fig. 13(d) shows the measured extra offset of the phase center of the antenna versus distance to the disk. For the distance exceeding about a quarter of the wavelength, the extra offset does not exceed 1 mm.

5. POTENTIALS FOR MM-PRECISION OF POSITIONING IN REAL TIME

The respective antennas are to approach the curve 3 of Fig. 1. So far, a vertical array antenna has been presented in [22]. The antenna exceeds 2 meters in height and is intended as a ground base for unmanned aircraft landing. Reference station antenna with a capacitive impedance ground plane of 3 meters in diameter is presented in [1, 23]. With this antenna, the multipath error falls below phase noise of the system. Perspectives of employing the antenna for CORS reference stations of the International GNSS Service (IGS) are discussed in [24]. However, dimensions of the antennas of above are substantial in wavelength scale. Further developments in the direction [25] show

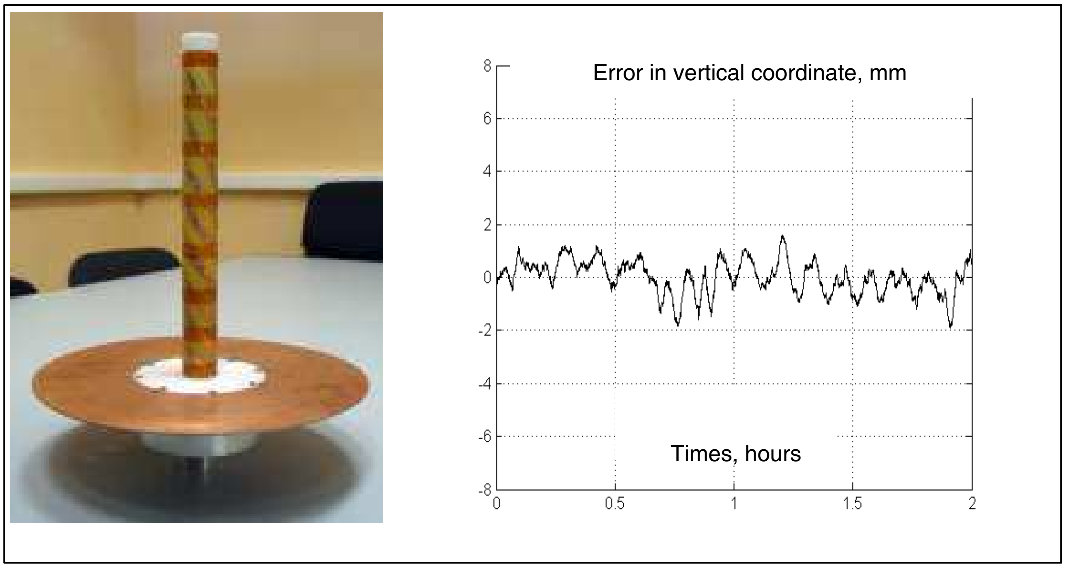

(a) (b)

Figure 14: Travelling wave helix antenna with cutoff pattern.

that competitive performance could be achieved with travelling wave helix antennas of about 1.5 wavelength height. An antenna sample is shown at the left panel of Fig. 14. The right panel illustrates the remaining multipath error to positioning in real time, with the noise being smoothed by a moving window of 1 minute span. The rms of the error is estimated as of 0.65 mm. One would mention that with such antennas it is no longer multipath that is the major error contribution but rather the phase noise.

6. CONCLUSION

Different kinds of antennas for high precision positioning developed at Topcon Center of Technology have been discussed. Newly developed compact rover antennas, field reference station antennas and antennas with cutoff pattern are presented. One would mention that with high precision applications so far, the antenna noise factor is to be kept at minimal levels. The newly developed antennas with cutoff patterns of moderate size potentially bring the mm precision in "almost" real time into the realm of practice.

REFERENCES

1. Leick, A., L. Rapoport, and D. Tatarnikov, *GPS Satellite Surveying*, 4th Edition, Wiley, New York, 2015.
2. Rao, B. R., W. Kunysz, P. Fante, and K. McDonald, *GPS/GNSS Antennas*, Artech House, Norwood, 2013.
3. Chen, X., C. G. Parini, B. Collins, Y. Yao, and M. U. Rehman, *Antennas for Global Navigation Satellite Systems*, Wiley, New York, 2012.
4. Garg, R., P. Bhartia, I. Bahl, and A. Ittipiboon, *Microstrip Antenna Design Handbook*, Artech House, Norwood, 2001.
5. Tatarnikov, D., "Patch antennas with artificial dielectric substrates," *Antennas*, Vol. 1, No. 128, 35–45, Radiotechnika, Moscow, 2008 (in Russian).
6. Tatarnikov, D., "Enhanced bandwidth patch antennas with artificial dielectrics substrates for high precision satellite positioning," *IWAT IEEE International Workshop on Antenna Technology, Small Antennas and Novel Metamaterials*, Santa-Monica, CA, Mar. 2009.
7. Silin, R. A. and V. P. Sazonov, *Slow-wave Structures*, National Lending Library for Science and Technology, Boston Spa Eng., 1971.
8. Tatarnikov, D., A. Astakhov, P. Shamatulsky, I. Soutiaguine, and A. Stepanenko, "Patch antenna with comb substrate," U.S. Patent 7,710,324 B2, 2008.
9. Tatarnikov, D., A. Astakhov, A. Stepanenko, and P. Shamatulsky, "Patch antenna with capacitive elements," U.S. Patent 8,446,322 B2, 2013.

10. Tretyakov, S., *Analytical Modeling in Applied Electromagnetics*, Artech House, Norwood, 2003.
11. Soutiaguine, I., D. Tatarnikov, A. Astakhov, V. Fillipov, and A. Stepanenko, "Antenna structures for reducing the effects of multipath radio signals," U.S. Patent 6,836,247 B2, 2004.
12. Tatarnikov, D., I. Soutiaguine, V. Filippov, A. Astakhov, A. Stepanenko, and P. Shamatulsky, "Multipath mitigation by conventional antennas with ground planes and passive vertical structures," *GPS Solutions*, Vol. 9, No. 3, 194–201, 2005.
13. Tatarnikov, D., A. Astakhov, and P. Shamatulsky, "Compact dual frequency RTK antennas," *Proc. of the 24-th Int. Tech. Meeting of the Institute of Navigation (ION GNSS 2011)*, 1179–1182, Sep. 20–23, 2011.
14. Tatarnikov, D., P. Shamatulsky, and A. Astakhov, "Compact multipath-resistant antenna system with integrated navigation receiver," U.S. Patent 8,842,045 B2, 2014.
15. Rabemanantsoa, J. and A. Sharaiha, "Size reduced multi-band printed quadrifilar helical antenna," *IEEE Trans. AP*, Vol. 59, No. 9, 3138–3143, 2011.
16. Tranquilla, J. M., J. P. Carr, and H. M. Al-Rizzo, "Analysis of a choke ring ground plane for multipath control in global positioning system (GPS) applications," *IEEE Trans. AP*, Vol. 42, No. 7, 905–911, 1994.
17. Kunysz, W., "A three dimensional choke ring ground plane antenna," *Proc. of the Institute of Navigation ION GNSS 2003*, 1883–1888, 2003.
18. Tatarnikov, D., A. Astakhov, and A. Stepanenko, "GNSS reference station antenna with convex impedance ground plane: Basics of design and performance characterization," *Proc. of the Int. Tech. Meeting of the Institute of Navigation ION ITM 2011*, 1240–1245, 2011.
19. Tatarnikov, D., A. Astakhov, and A. Stepanenko, "Broadband convex ground planes for multipath rejection," U.S. Patent 8,441,409 B2, 2013.
20. Tatarnikov, D., "Semi-transparent ground planes excited by magnetic line current," *IEEE Trans. AP*, Vol. 60, No. 6, 2843–2852, 2012.
21. Dilssner, F., G. Seeber, G. Wübbena, and M. Schmitz, "Impact of near-field effects on the GNSS position solution," *Proc. ION GNSS 2008*, 612–624, Institute of Navigation, 2008.
22. Lopez, A. R., "GPS landing system reference antenna," *IEEE Antennas and Propagation Magazine*, Vol. 52, No. 1, 105–113, 2010.
23. Tatarnikov, D. and A. Astakhov, "Large impedance ground plane antennas for MM-accuracy of GNSS positioning in real time," *PIERS Proceedings*, 1825–1829, Stockholm, Aug. 12–15, 2013.
24. Mader, G. L., A. Bilich, and D. Tatarnikov, "BigAnt: Engineering and experimental results," *IGS Workshop*, Pasadena, 2014.
25. Tatarnikov, D. and I. Chernetsky, "Travelling-wave antennas with semitransparent surfaces for forming a cutoff pattern," *PIERS Proceedings*, Prague, Czech Republic, accepted for presentation, 2015.